Inorg. Chem. **2006**, *45*, 4820−4829

Photoinduced Energy Transfer Coupled to Charge Separation in a Ru(II)−Ru(II)−Acceptor Triad

Magnus Borgström,[†] Sascha Ott,[†] Reiner Lomoth,[†] Jonas Bergquist,[‡] Leif Hammarström,*[,†] and Olof Johansson*[,†]

Department of Photochemistry and Molecular Science, BMC, Uppsala University, BOX 579, 751 23 Uppsala, Sweden, and Department of Physical and Analytical Chemistry, Analytical Chemistry, BMC, Uppsala University, BOX 599, 751 24 Uppsala, Sweden

Received January 20, 2006

The bichromophoric system Ru–Ru_C–PI ([(bpy)$_3$Ru–Ph–Ru(dpb)(Metpy-PI)][PF_6]$_3$, where bpy is 2,2′-bipyridine, Hdpb is 1,3-di(2-pyridyl)-benzene, Metpy is 4′-methyl-2,2′:6′,2″-terpyridine and PI is pyromellitimide) containing two Ru(II) polypyridyl chromophores with a N_6 and a N_5C ligand set, respectively, was synthesized and characterized. Its photophysical properties were investigated and compared to those of the monochromophoric cyclometalated complexes Ru_C–PI ([Ru(dpb)(Metpy-PI)][PF_6]), Ru_C–φ–PI ([Ru(dpb)(ttpy-PI)][PF_6], ttpy is 4′-*p*-tolyl-2,2′:6′,2″-terpyridine), Ru_C–φ ([Ru(dpb)(ttpy)][PF_6]), and Ru_C ([Ru(dpb)(Metpy)][PF_6]). Excitation of the Ru_C unit in the dyads leads to oxidative quenching, forming the Ru_C^{III}–φ–$PI^{\bullet-}$ and Ru_C^{III}–$PI^{\bullet-}$ charge-separated (CS) states with $k_{ET}^f = 7.7 \times 10^7$ s^{-1} (CH_3CN, 298 K) in the tolyl-linked Ru_C–φ–PI and $k_{ET}^f = 4.4 \times 10^9$ s^{-1} (CH_2Cl_2, 298 K) in the methylene-linked Ru_C–PI. In the Ru–Ru_C–PI triad, excitation of the Ru_C chromophore leads to dynamics similar to those in the Ru_C–PI dyad, generating the Ru^{II}–Ru_C^{III}–$PI^{\bullet-}$ CS state, whereas excitation of the Ru unit results in an initial energy transfer ($k_{EnT} = 4.7 \times 10^{11}$ s^{-1}) to the cyclometalated Ru_C unit. Subsequent electron transfer to the PI acceptor results in the formation of the same Ru^{II}–Ru_C^{III}–$PI^{\bullet-}$ CS state with $k_{ET}^f = 5.6 \times 10^9$ s^{-1} that undergoes rapid recombination with $k_{ET}^b = 1 \times 10^{10}$ s^{-1} (CH_2Cl_2, 298 K). The fate of the Ru^{II}–Ru_C^{III}–$PI^{\bullet-}$ CS state upon a second photoexcitation was studied by pump–pump–probe experiments in an attempt to detect the fully charge-separated Ru^{III}–Ru_C^{II}–$PI^{\bullet-}$ state.

Introduction

The unique processes of photosynthesis in which light energy is converted into chemical energy have inspired scientists to create synthetic analogues for a long time. Many molecules capable of performing light-induced charge separation have been synthesized and studied in detail.[1−6] The most-common design of such devices consists of covalently linked assemblies based on a single photosensitizer (P). With visible light, excited state energies are typically around 2 eV; the energy of the charge-separated (CS) state rarely exceeds 1.5 eV in common donor−sensitizer−acceptor (D−P−A) systems and is typically much smaller. An ultimate challenge in the field is to use this energy to split water into hydrogen and oxygen. Because the free energy change for this process is rather high (1.23 eV), it would be advantageous to increase the energy of the photoinduced CS state in order to drive the catalytic redox reactions of water oxidation and proton reduction at suitable catalytic sites. One strategy for achieving this is to use two photosensitizers instead of one, in a D−P_1−P_2−A assembly. Such a system could use the energy of two low-energy photons to create a high-energy CS state by optimizing each photosensitizer

* To whom correspondence should be addressed. E-mail: olof.johansson@fotomol.uu.se.
[†] Department of Photochemistry and Molecular Science, Uppsala University.
[‡] Department of Physical and Analytical Chemistry, Uppsala University.

(1) Huynh, M. H. V.; Dattelbaum, D. M.; Meyer, T. J. *Coord. Chem. Rev.* **2005**, *249*, 457−483.
(2) Baranoff, E.; Collin, J.-P.; Flamigni, L.; Sauvage, J.-P. *Chem. Soc. Rev.* **2004**, *33*, 147−155.
(3) Imahori, H.; Mori, Y.; Matano, Y. *J. Photochem. Photobiol., C* **2003**, *4*, 51−83.
(4) Gust, D.; Moore, T. A.; Moore, A. L. *Acc. Chem. Res.* **2001**, *34*, 40−48.
(5) Gust, D.; Moore, T. A.; Moore, A. L. Covalently Linked Systems Containing Porphyrin Units. In *Electron Transfer in Chemistry*; Balzani, V., Ed.; Wiley-VCH: Weinheim, Germany, 2001; pp 272−336.
(6) Wasielewski, M. R. *Chem. Rev.* **1992**, *92*, 435−461.

10.1021/ic060121l CCC: $33.50
Published on Web 05/16/2006

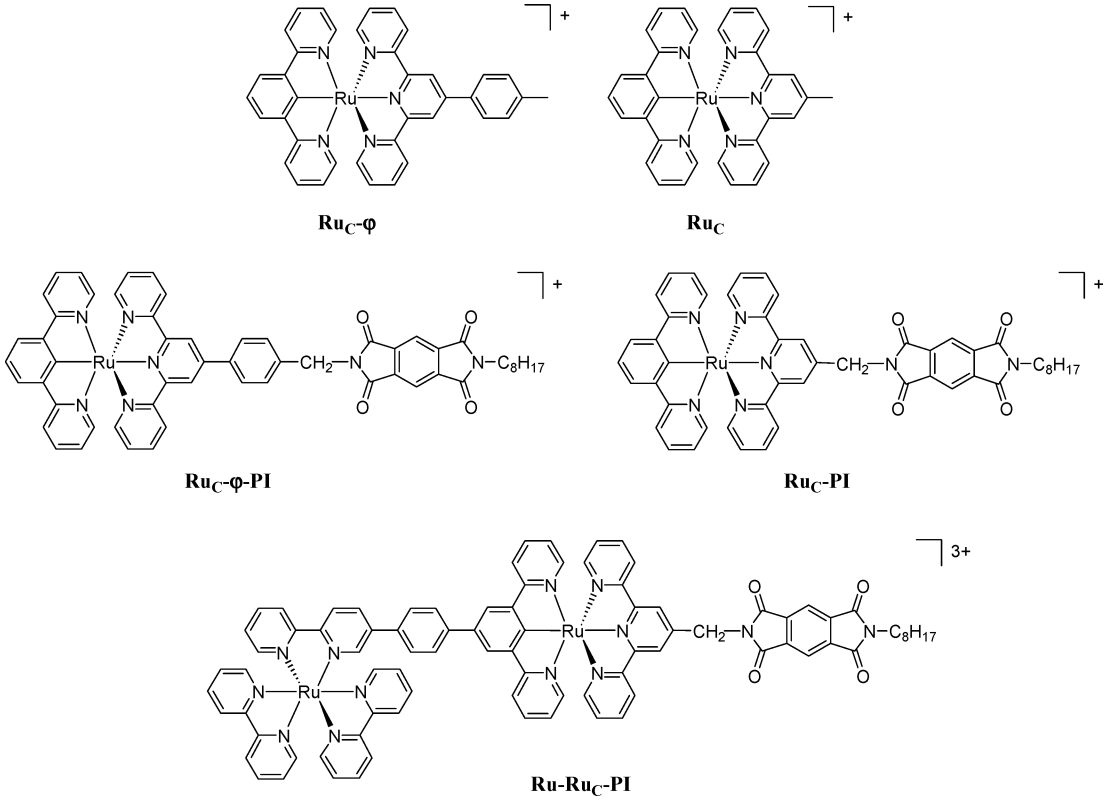

Figure 1. Structures of complexes.

independently, providing a maximum of oxidation and reduction power. When only one single photosensitizer is used, its electrochemical properties will likely be a compromise. Note that this strategy differs from previous work containing multiple photosensitizer donor−acceptor systems[7−9] in that both chromophores would be involved in the charge-separation process.

In a previous study, we thoroughly investigated the interaction between the ruthenium units in two Ru−(bridge)−Ru$_C$ dyads where we demonstrated fast-exchange energy transfer from the tris-bipyridyl (Ru) to the cyclometalated (Ru$_C$) unit on an ∼1 ps time scale.[10] We have now set out to exploit this process and couple the observed energy-transfer event to further charge separation in a first attempt toward our main goal of achieving high-energy CS states. $[Ru(bpy)_3]^{2+}$ (bpy is 2,2′-bipyridine) was chosen as the P_1 unit because of the high potential of the $Ru^{III/II}$ redox couple[11] ($E_{1/2}$ = 0.88 V vs $Fc^{+/0}$). For a P_2 unit, the cyclometalated $[Ru(dpb)(ttpy)]^{+}$ [12] (Hdpb is 1,3-di(2-pyridyl)-benzene and ttpy is 4′-*p*-tolyl-2,2′:6′,2″-terpyridine) was employed, where the anionic dpb^- ligand reduces the reduction potential of the excited state ($E_{1/2} = -1.53$ V vs $Fc^{+/0}$) compared to that of $[Ru(bpy)_3]^{2+}$ ($E_{1/2} = -1.24$ V vs $Fc^{+/0}$).[13] This allows us to employ pyromellitimide (PI) as the electron acceptor with a more-negative reduction potential ($E_{1/2} \approx -1.2$ V vs $Fc^{+/0}$)[14,15] compared to the more commonly used naphthalenediimide (NDI) acceptor ($E_{1/2} \approx -0.95$ V vs $Fc^{+/0}$).[15−17] The design of the P_1-P_2-A triad Ru−Ru$_C$−PI (Figure 1) on the basis of a heteroleptic cyclometalated Ru$_C$ unit with bis-tridentate ligands avoids the common problem of structural isomers when combining several ruthenium polypyridyl units.[18]

In this work, we present the synthesis, characterization, and photophysical properties of the novel Ru$_C$−PI, Ru$_C$−

(7) (a) Konduri, R.; de Tacconi, N. R.; Rajeshwar, K.; MacDonnell, F. M. *J. Am. Chem. Soc.* **2004**, *126*, 11621−11629. (b) Konduri, R.; Ye, H.; MacDonnell, F. M.; Serroni, S.; Campagna, S.; Rajeshwar, K. *Angew. Chem., Int. Ed.* **2002**, *41*, 3185−3187.
(8) (a) Swavey, S.; Brewer, K. J. *Inorg. Chem.* **2002**, *41*, 4044−4050. (b) Molnar, S. M.; Nallas, G.; Bridgewater, J. S.; Brewer, K. J. *J. Am. Chem. Soc.* **1994**, *116*, 5206−5210.
(9) (a) Kodis, G.; Liddell, P. A.; de la Garza, L.; Clausen, P. C.; Lindsey, J. S.; Moore, A. L.; Moore, T. A.; Gust, D. *J. Phys. Chem. A* **2002**, *106*, 2036−2048. (b) Kuciauskas, D.; Liddell, P. A.; Lin, S.; Johnson, T. E.; Weghorn, S. J.; Lindsey, J. S.; Moore, A. L.; Moore, T. A.; Gust, D. *J. Am. Chem. Soc.* **1999**, *121*, 8604−8614.
(10) Ott, S.; Borgström, M.; Hammarström, L.; Johansson, O. *Dalton Trans.* **2006**, 1434−1443.
(11) Juris, A.; Balzani, V.; Barigelletti, F.; Campagna, S.; Belser, P.; von Zelewsky, A. *Coord. Chem. Rev.* **1988**, *84*, 85−277.
(12) (a) Beley, M.; Chodorowski, S.; Collin, J.-P.; Sauvage, J.-P.; Flamigni, L.; Barigelletti, F. *Inorg. Chem.* **1994**, *33*, 2543−2547. (b) Beley, M.; Collin, J.-P.; Sauvage, J.-P. *Inorg. Chem.* **1993**, *32*, 4539−4543.
(13) Calculated from the Weller equation: $E^0(Ru^{3+/2+*}) = E^0(Ru^{3+/2+}) - E_{00}/e$) on the basis of an excited-state energy of E_{00} = 1.63 eV and E_{00} = 2.12 eV for $[Ru(dpb)(ttpy)]^+$ and $[Ru(bpy)_3]^{2+}$, respectively.
(14) (a) Gosztola, D.; Niemczyk, M. P.; Svec, W. A.; Lucas, A. S.; Wasielewski, M. R. *J. Phys. Chem. A* **2000**, *104*, 6545−6551. (b) Lukas, A. S.; Miller, S. E.; Wasielewski, M. R. *J. Phys. Chem. B* **2000**, *104*, 931−940.
(15) Hossain, D.; Haga, M.; Monjushiro, H.; Gholamkhass, B.; Nozaki, K.; Ohno, T. *Chem. Lett.* **1997**, 573−574.
(16) (a) Borgström, M.; Shaikh, N.; Johansson, O.; Anderlund, M. F.; Styring, S.; Åkermark, B.; Magnuson, A.; Hammarström, L. *J. Am. Chem. Soc.* **2005**, *127*, 17504−17515. (b) Johansson, O.; Wolpher, H.; Borgström, M.; Hammarström, L.; Bergquist, J.; Sun, L.; Åkermark, B. *Chem. Commun.* **2004**, 194−195. (c) Johansson, O.; Borgström, M.; Lomoth, R.; Palmblad, M.; Bergquist, J.; Hammarström, L.; Sun, L.; Åkermark, B. *Inorg. Chem.* **2003**, *42*, 2908−2918.
(17) Dixon, D. W.; Thornton, N. B.; Steullet, V.; Netzel, T. *Inorg. Chem.* **1999**, *38*, 5526−5534.
(18) Keene, F. R. *Coord. Chem. Rev.* **1997**, *166*, 121−159.

φ−PI, and Ru−Ru_C−PI complexes. From the investigation of the primary charge separation in the monochromophoric Ru_C−PI and Ru_C−φ−PI models, it became apparent that the shorter methylene link provides superior electron-transfer properties, which led to the design of the Ru−Ru_C−PI triad. The primary charge-separation step in the Ru−Ru_C−PI triad (P_1−*P_2−A → P_1−$P_2^{\bullet+}$−$A^{\bullet-}$) was shown to occur regardless of excitation wavelength. We also explored the possibility of generating the high-energy Ru^{III}−Ru_C^{II}−$PI^{\bullet-}$ state via the absorption of a second photon by the primary Ru^{II}−Ru_C^{III}−$PI^{\bullet-}$ CS state (*P_1−$P_2^{\bullet+}$−$A^{\bullet-}$→ $P_1^{\bullet+}$−P_2−$A^{\bullet-}$). For this purpose, we used the pump−pump−probe technique earlier adapted by Wasielewski and co-workers, who had a different goal of achieving molecular switches.[19]

Experimental Section

HPLC-MS data were obtained on a Gilson system on a Phenomenex Gemini C18 column (150 × 3 mm, 5 μm) coupled to a Finnigan AQA Thermo Quest with electrospray ionization (ESI-MS). Solvents used for HPLC were 0.1% HCO_2H in H_2O and 0.1% HCO_2H in CH_3CN. Mass spectrometry experiments were done on a high-resolution Bruker Daltonics BioAPEX-94e superconducting 9.4 T FTICR mass spectrometer (Bruker Daltonics, Billerica, MA) (ESI−FTICR MS) equipped with an in-house-developed emitter.[20]

Spectroscopy. ^{1}H NMR spectra were recorded on a Varian (300 or 400 MHz) spectrometer. UV−vis absorption spectra were measured on a Hewlett−Packard 8453 instrument. Fluorescence spectra were recorded on a SPEX Fluoromax fluorimeter and were corrected for the wavelength-dependent response of the detector system.

Time-resolved correlated single photon counting measurements were performed on a previously described system.[16c] The emission was collected at magic angle polarization (55.4°) relative to the excitation light, and the instrument had a response function with a fwhm of ∼60 ps. The concentration of the samples in the emission experiments was controlled so that the absorption at the pump wavelength was held around 0.1.

The laser pulses generated for the transient absorption pump−probe experiments have been previously described.[21] The 800 nm output was converted to 450 or 550 nm, with a temporal width of ∼150 fs, in an optical parametric amplifier (TOPAS). A mechanical chopper blocked every second pump beam. The probe light was passed through a moveable delay line, allowing the delay between pump and probe to vary as much as 10 ns. A vertically moving CaF_2 crystal in the probe beam produced a continuous white light and a $\lambda/2$ plate adjusted the polarization of the light so that the difference in polarization between pump and probe was fixed at magic angle conditions. The pump and probe beam was then focused in a vertically moving 1 × 10 mm^2 cell. The transmitted probe light was divided spatially on an optical diffraction grating and further detected on a diode array. To adjust for differences in laser intensity, we passed parts of the probe light to the detector without passing the sample and the transient absorption was calculated as $\Delta abs = -\log[(I_{probe,\tau=t}/I_{reference,\tau=t})/(I_{probe,\tau=0}/I_{reference,\tau=0})]$. The reported values are averages of 5000−10 000 individual measurements. For the single-pump experiments, the pump energy was set below 2 μJ. In the pump−pump−probe experiments, the 450 nm pump was split in a 70/30 ratio by a beam splitter. The high-energy part was focused directly on the sample, whereas the low-energy part focused on the sample after passing a second delay line. To allow for maximum transient signals, we set the total pump energy in the pump−pump−probe experiments at 3.5 μJ. With this energy, no severe sample degradation was observed.

For the experiments on Ru_C−PI, we performed an estimate of the solvent dependence on the free energy driving force on the basis of the electrochemical data in CH_3CN. In the equations below, the donor and acceptor units are treated as spheres.[22]

$$\Delta G_{CR}^0 = (E_{1/2}^{PI^{0/-}} - E_{1/2}^{Ru_C{}^{2+/+}})_{CH_3CN} - \frac{e^2}{4\pi\epsilon_0}\left[\left(\frac{1}{\epsilon_{solv}} - \frac{1}{\epsilon_{CH_3CN}}\right) \times \left(\frac{Z_{p_1} - Z_{r_1}}{2a_1} + \frac{Z_{p_2} - Z_{r_2}}{2a_2}\right) - \frac{Z_{p_1}Z_{p_2}}{\epsilon_{solv}r}\right] \quad (1)$$

$$\Delta G_{CS}{}^0 = -E_{Ru_C}^{00} + -\Delta G_{CR}^0 \quad (2)$$

$E_{1/2}$ is the halfwave potential and ϵ is the static dielectric constant. Z is the charge number of the donor and the acceptor in the ground (Z_r) and charge-separated (Z_p) states. a_1 and a_2 are the radii of the redox units and r is the distance between the components. For the Ru_C−PI dyad, we used the following values: $a_1 = 7$ Å (Ru), $a_2 = 5$ Å (PI), and $r = 10$ Å. In eq 1, the first term in the square brackets gives the contribution from the Born solvation energy in a specific solvent as compared to the solvent used for the determination of the $E_{1/2}$ values. The second term gives the contribution from the coulombic interaction stabilizing the CS state.

Electrochemistry. Cyclic voltammetry was carried out with a three-electrode setup in a three-compartment cell connected to an Autolab potentiostat with a GPES electrochemical interface (Eco Chemie). The working electrode was a glassy carbon disk (diameter 3 mm, freshly polished). Potentials were measured vs a nonaqueous Ag/Ag^+ reference electrode (CH Instruments, 10 mM $AgNO_3$ in acetonitrile) with a potential of −0.080 V vs the ferrocenium/ferrocene ($Fc^{+/0}$) couple in acetonitrile. All potentials reported here are referenced vs the $Fc^{+/0}$ couple by adding −0.080 V to the potentials measured vs the Ag/Ag^+ electrode. Solutions were prepared from dry acetonitrile (Merck, spectroscopy grade, dried with MS 3 Å) and contained ca. 1 mM of the analyte and 0.1 M tetrabutylammonium hexafluorophosphate (Fluka, electrochemical grade, dried at 373 K) as the supporting electrolyte. The glassware used was oven dried, assembled, and flushed with argon while hot. Before all measurements, oxygen was removed by bubbling the stirred solutions with solvent-saturated argon; the samples were kept under an argon atmosphere during measurements.

Synthesis. All solvents and reagents were used as received from commercial suppliers unless otherwise noted. 4′-[4-(Aminomethyl)-phenyl]-2,2′:6′,2″-terpyridine (**1**),[16c] pyridacyl pyridinium iodide (**10**),[23] 4′-methyl-2,2′:6′,2″-terpyridine (Metpy),[24] 1,3-di(2-pyridyl)-benzene (Hdpb),[12a] Ru_C−φ,[12a] and [(bpy)$_3$Ru−Ph-Hdpb][PF_6]$_2$[10]

(19) (a) Andersson, M.; Sinks, L. E.; Hayes, R. T.; Zhao, Y.; Wasielewski, M. R. *Angew. Chem., Int. Ed.* **2003**, *27*, 3139−3143. (b) Lukas, A. S.; Bushard, P. J.; Wasielewski, M. R. *J. Am. Chem. Soc.* **2001**, *123*, 2440−2441. (c) Hayes, R. T.; Wasielewski, M. R.; Gosztola, D. *J. Am. Chem. Soc.* **2000**, *122*, 5563−5567. (d) Debreczeny, M. P.; Svec, W. A.; Marsh, E. M.; Wasielewski, M. R. *J. Am. Chem. Soc.* **1996**, *118*, 8174−8175.

(20) Nilsson, S.; Wetterhall, M.; Bergquist, J.; Nyholm, L.; Markides, K. *Rapid Commun. Mass Spectrom.* **2001**, *15*, 1997−2000.

(21) Andersson, M.; Davidsson, J.; Hammarström, L.; Korppi-Tommola, J.; Peltola, T. *J. Phys. Chem. B* **1999**, *103*, 3258−3262.

(22) Rehm, D.; Weller, A. *Isr. J. Chem.* **1970**, *8*, 259−271.

(23) Priimov, G. U.; Moore, P.; Maritim, P. K.; Butalanyi, P. K.; Alcock, N. W. *J. Chem. Soc., Dalton Trans.* **2000**, 445−449.

(24) Johansson, A.; Abrahamsson, M.; Magnuson, A.; Huang, P.; Mårtensson, J.; Styring, S.; Hammarström, L.; Sun, L.; Åkermark, B. *Inorg. Chem.* **2003**, *42*, 7502−7511.

were prepared as described previously. *N*-(2-Ethylhexyl)-benzene-1,2-dicarboxanhydride-4,5-dicarboximide (**2**) was prepared as described for *N*-octylbenzene-1,2-dicarboxanhydride-4,5-dicarboximide.[25] $Ru(Metpy)Cl_3$, $Ru(ttpy\text{-}PI)Cl_3$, and $Ru(Metpy\text{-}PI)Cl_3$ were prepared in manner similar to that for $Ru(tpy)Cl_3$[26] and used without further purification.

Terpyridine 3 (ttpy-PI). 4′-[4-(Aminomethyl)phenyl]-2,2′:6′,2″-terpyridine (**1**) (0.749 g, 2.21 mmol) and *N*-(2-ethylhexyl)-benzene-1,2-dicarboxanhydride-4,5-dicarboximide (**2**) (0.780 g, 2.37 mmol) were refluxed in freshly distilled toluene (40 mL) under nitrogen for 12 h. The clear solution was allowed to reach room temperature. Hexane (40 mL) was added, and the resulting precipitate was filtered off, washed with cold toluene/hexane (1:1), and subsequently dried under vacuum (1.13 g, 78%). ^{1}H NMR (300 MHz, $CDCl_3$, 25 °C): δ 0.85−1.00 (m, 6H), 1.20−1.40 (m, 8H), 1.85 (m, 1H), 3.63 (d, 2H), 4.97 (s, 2H), 7.36 (ddd, 1H), 7.59 (d, 2H), 7.85−7.94 (m, 4H), 8.29 (s, 2H), 8.67 (d, 2H), 8.70−8.75 (m, 4H). ^{13}C NMR: δ 10.5, 14.2, 23.1, 24.0, 28.6, 30.7, 38.4, 42.1, 42.7, 118.5, 119.0, 121.5, 124.0, 127.9, 129.5, 136.5, 137.0, 137.3, 137.4, 138.6, 149.2, 149.7, 156.1, 156.2, 166.0, 166.6.

***N*-(Acetaldehyde dimethyl acetal)-*N*′-(2-ethylhexyl)-benzene-1,2,4,5-tetra-carboxydiimide 5.** Aminoacetaldehyde dimethyl acetal (**4**) (0.178 g, 1.70 mmol) and *N*-(2-ethylhexyl)-benzene-1,2-dicarboxanhydride-4,5-dicarboximide (**2**) (0.526 g, 1.60 mmol) were refluxed in freshly distilled toluene under a nitrogen atmosphere for 22 h. The solvent was removed, and the residue was chromatographed on silica gel (eluent, 1:2 EtOAc:toluene) to give **5** (0.429 g, 64%). ^{1}H NMR (300 MHz, $CDCl_3$, 25 °C): δ 0.85−1.00 (m, 6H), 1.20−1.40 (m, 8H), 1.85 (m, 1H), 3.38 (s, 6H), 3.64 (d, 2H), 3.88 (d, 2H), 4.77 (t, 1H), 8.28 (s, 2H). ^{13}C NMR: δ 10.6, 14.2, 23.2, 24.1, 28.7, 30.7, 38.5, 39.5, 42.8, 53.5, 100.0, 118.5, 137.3, 137.5, 166.2, 166.7.

***N*-Acetaldehyde-*N*′-(2-ethylhexyl)-benzene-1,2,4,5-tetracarboxydiimide 6.** Compound **5** (0.985 g, 2.36 mmol) was dissolved in a 1:1 $CHCl_3$:CF_3COOH mixture (16 mL) and stirred at room temperature for 4 h. Saturated $NaHCO_3$ was added until neutral pH was reached. The mixture was extracted with $CHCl_3$, and the organic phase was dried over Na_2SO_4. After the solvent was removed, compound **6** was isolated as a white solid (0.853 g, 97%). ^{1}H NMR (300 MHz, $CDCl_3$, 25 °C): δ 0.85−1.00 (m, 6H), 1.20−1.40 (m, 8H), 1.85 (m, 1H), 3.65 (d, 2H), 4.65 (s, 2H), 8.31 (s, 2H), 9.67 (s, 1H). ^{13}C NMR: δ 10.6, 14.2, 23.2, 24.1, 28.7, 30.7, 38.5, 42.9, 48.0, 118.8, 137.2, 137.7, 165.6, 166.6, 192.4.

Compound 8. 2-Acetylpyridine (0.230 mL, 1.96 mmol) was added dropwise to a THF (distilled from Na/benzophenone) solution (5 mL) of LDA (2.1 mmol) at −50 °C. After 40 min, the solution was subsequently transferred dropwise to a solution of **6** (0.699 g, 1.89 mmol) in THF (20 mL) at −78 °C. The solution was brought to room temperature after 30 min, after which saturated NH_4Cl was added. The organic phase was separated, and the water phase was extracted with Et_2O. The combined organic phases were dried over Na_2SO_4, and the solvent was removed. The residue was chromatographed on silica (eluent, 1:2 EtOAc:toluene) to give **8** (0.211 g, 23%). ^{1}H NMR (300 MHz, $CDCl_3$, 25 °C): δ 0.85−1.00 (m, 6H), 1.20−1.40 (m, 8H), 1.85 (m, 1H), 3.39 (dd, 1H), 3.48 (dd, 1H), 3.63 (d, 2H), 3.86 (dd, 1H), 4.02 (dd, 1H), 4.53 (m, 1H), 7.52 (ddd, 1H), 7.88 (dt, 1H), 8.06 (m, 1H), 8.28 (s, 2H), 8.66 (m, 1H). ^{13}C NMR: δ 10.6, 14.2, 23.2, 24.1, 28.7, 30.7, 38.5, 42.8, 43.4, 44.1, 66.3, 118.5, 122.5, 127.9, 137.4, 137.5, 137.7, 149.0, 152.9, 166.6, 166.8, 200.5.

Compound 9. Compound **8** (0.210 g, 0.43 mmol) was dissolved in dry CH_2Cl_2 (8 mL), and the temperature was reduced to −30 °C. Triethylamine (0.16 mL, 1.1 mmol) was added, followed by a dropwise addition of methanesulfonyl chloride (0.040 mL, 0.50 mmol). The solution was allowed to reach room temperature and was left overnight. The solution was washed with H_2O and dried over Na_2SO_4. After the solvent was removed, the residue was chromatographed on silica (eluent, 1:2 EtOAc:toluene) to give enone **9** (0.120 g, 59%). ^{1}H NMR (300 MHz, $CDCl_3$, 25 °C): δ 0.85−1.00 (m, 6H), 1.20−1.40 (m, 8H), 1.86 (m, 1H), 3.64 (d, 2H), 4.64 (d, 2H), 7.12 (dt, 1H), 7.48 (ddd, 1H), 7.78 (d, 1H), 7.85 (dt, 1H), 8.11 (d, 1H), 8.31 (s, 2H), 8.66 (m, 1H). ^{13}C NMR: δ 10.6, 14.2, 23.1, 24.1, 28.6, 30.7, 38.5, 39.7, 42.8, 118.6, 123.2, 126.6, 127.4, 137.2, 137.3, 137.6, 140.0, 149.1, 153.5, 165.8, 166.7, 188.9.

Terpyridine 11 (Metpy-PI). Pyridacyl pyridinium iodide (**10**) (0.108 g, 0.33 mmol), enone **9** (0.155 g, 0.33 mmol), and NH_4OAc (0.46 g, 6 mmol) were heated in MeOH (2 mL) at reflux under N_2 for 8 h. The formed solid was filtered off and washed with additional MeOH until the washings were colorless, giving **11** as an off-white solid (0.055 g, 29%). ^{1}H NMR (300 MHz, $CDCl_3$, 25 °C): δ 0.85−1.00 (m, 6H), 1.20−1.40 (m, 8H), 1.84 (m, 1H), 3.62 (d, 2H), 5.08 (s, 2H), 7.33 (ddd, 2H), 7.84 (dt, 2H), 8.29 (s, 2H), 8.45 (s, 2H), 8.57 (d, 2H), 8.67 (m, 2H). ^{13}C NMR: δ 10.6, 14.2, 23.2, 24.1, 28.7, 30.7, 38.5, 41.8, 42.8, 118.7, 120.3, 121.6, 124.2, 137.2, 137.4, 137.6, 146.4, 149.2, 155.8, 156.2, 166.1, 166.7.

4′-Cyano-2,2′:6′,2″-terpyridine 13. 4′-Chloro-2,2′:6′,2″-terpyridine (0.075 g, 0.28 mmol), $Zn(CN)_2$ (0.020 g, 0.17 mmol), Zn (0.005 g, 0.08 mmol), $Pd(dba)_2$ (0.007 g, 0.01 mmol), and dppf (0.015 g, 0.03 mmol) in DMA (1.5 mL) were heated at 180 °C using microwave heating for 75 min. The DMA was removed; the residue was suspended in $CHCl_3$ and filtered through Celite and a short alumina (activated, neutral) column to give **13** (0.047 g, 65%). ^{1}H NMR (300 MHz, $CDCl_3$, 25 °C): 7.43 (ddd, 2H), 7.92 (dt, 2H), 8.63 (m, 2H), 8.74 (s, 2H), 8.76 (m, 2H). HPLC ESI-MS (*m*/*z*): ($M + H^+$) 259.3 (calcd, 259.1).

4′-Aminomethyl-2,2′:6′,2″-terpyridine 14. 4′-Cyano-2,2′:6′,2″-terpyridine (0.035 g, 0.14 mmol) and 10% Pd/C (0.005 g) were added to AcOH and stirred under H_2 (1 atm) for 24 h. The mixture was filtered through Celite; the solvent was removed, and the residue was treated with saturated $NaHCO_3$ and subsequently extracted with $CHCl_3$. After being dried over Na_2SO_4, the solvent was removed to give **14** (0.030 g, 84%). ^{1}H NMR (300 MHz, $CDCl_3$, 25 °C): δ 4.07 (s, 2H), 7.34 (ddd, 2H), 7.87 (dt, 2H), 8.43 (s, 2H), 8.63 (d, 2H), 8.71 (m, 2H). ^{13}C NMR: δ 46.2, 119.4, 121.6, 124.0, 137.1, 149.3, 154.7, 155.9, 156.5.

Alternative Synthesis of 11. 4′-Aminomethyl-2,2′:6′,2″-terpyridine (0.020 g, 0.076 mmol) and *N*-(2-ethylhexyl)-benzene-1,2-dicarboxanhydride-4,5-dicarboximide (**2**) (0.028 g, 0.085 mmol) were refluxed in freshly distilled toluene (2.5 mL) under a nitrogen atmosphere for 24 h. The solution was concentrated to half the volume, and pentane was added. The formed precipitate was filtered off and washed with cold pentane (0.029 g, 67%). The NMR spectra were identical to those previously recorded for **11** (above).

$[Ru(dpb)(ttpy\text{-}PI)][PF_6]$ ($Ru_C-\varphi-PI$). $Ru(ttpy\text{-}PI)Cl_3$ (0.072 g, 0.084 mmol) and $AgBF_4$ (0.100 g, 0.51 mmol) were heated at reflux in acetone (20 mL) for 2 h. The formed AgCl was filtered off, and the acetone was removed in vacuo. The remaining purple residue was dissolved in a 1:1 mixture of DMF:*n*-BuOH (16 mL), and Hdpb (0.022 g, 0.095 mmol) was added. After the solution was stirred at 130 °C under N_2 for 4 h, the solvents were removed in vacuo and the residue was purified by column chromatography

(25) Wiederrecht, G. P.; Svec, W. A.; Niemczyk, M. P.; Wasielewski, M. R. *J. Phys. Chem.* **1995**, *99*, 8918−8926.
(26) Sullivan, B. P.; Calvert, J. M.; Meyer, T. J. *Inorg. Chem.* **1980**, *19*, 1404−1407.

on silica (eluent, 40:4:1 CH_3CN:H_2O(aq):KNO_3). After anion exchange with PF_6^-, the title complex was further purified on a short alumina column (activated neutral; eluent, 1:1 CH_3CN:toluene) and isolated as a dark purple solid (0.032 g, 33%). ^{1}H NMR (300 MHz, CD_3CN, 25 °C): δ 0.85−0.95 (m, 6H), 1.25−1.40 (m, 8H), 1.80 (m, 1H), 3.59 (d, 2H), 5.04 (s, 2H), 6.64 (ddd, 2H), 6.95 (ddd, 2H), 7.07 (m, 2H), 7.11 (m, 2H), 7.46 (t, 1H), 7.60 (m, 2H), 7.70 (m, 2H), 7.74 (d, 2H), 8.10−8.20 (m, 4H), 8.25−8.30 (m, 4H), 8.54 (m, 2H), 8.98 (s, 2H). ESI−FTICR MS (*m*/*z*): $[M - PF_6^-]^+$ 982.3 (calcd for $C_{56}H_{46}N_7O_4Ru$, 982.3). Elemental anal. Calcd (%) for $C_{56}H_{46}N_7O_4RuPF_6 \cdot 1H_2O$: C, 58.74; H, 4.23; N, 8.56. Found: C, 58.52; H, 4.26; N, 8.59.

[Ru(dpb)(Metpy-PI)][PF$_6$] (Ru$_C$−PI). Prepared the same way as [Ru(dpb)(ttpy-PI)][PF_6] above. Ru(Metpy-PI)Cl_3 (0.036 g, 0.046 mmol) and $AgBF_4$ (0.049 g, 0.25 mmol) in acetone (10 mL). Hdpb (0.013 g, 0.056 mmol) in 9:1 DMF:*n*-BuOH (8 mL). Purified by column chromatography on silica (eluent, 95:5:1 CH_3CN:H_2O(aq):KNO_3). Yield: 0.018 g, 37%. ^{1}H NMR (300 MHz, CD_3CN, 25 °C): δ 0.85−0.95 (m, 6H), 1.25−1.40 (m, 8H), 1.81 (m, 1H), 3.61 (d, 2H), 5.35 (s, 2H), 6.62 (ddd, 2H), 6.90−7.00 (m, 4H), 7.10 (m, 2H), 7.44 (t, 1H), 7.58 (m, 2H), 7.66 (dt, 2H), 8.12 (m, 2H), 8.24 (d, 2H), 8.35 (s, 2H), 8.41 (m, 2H), 8.71 (s, 2H). HPLC ESI-MS (*m*/*z*): $[M - PF_6^-]^+$ 906.9 (calcd for $C_{50}H_{42}N_7O_4Ru$, 906.2). Elemental anal. Calcd (%) for $C_{50}H_{42}N_7O_4RuPF_6$: C, 57.14; H, 4.03; N, 9.33. Found: C, 57.22; H, 4.20; N, 9.18.

[Ru(dpb)(Metpy][PF$_6$] (Ru$_C$). Prepared as described above. Ru(Metpy)Cl_3 (0.050 g, 0.11 mmol) and $AgBF_4$ (0.085 g, 0.44 mmol) in acetone (18 mL). Hdpb (0.033 g, 0.14 mmol) in 9:1 DMF:*n*-BuOH (14 mL). Purified by column chromatography on silica (eluent, 40:4:1 CH_3CN:H_2O(aq):KNO_3). Yield: 0.033 g, 41%. ^{1}H NMR (300 MHz, CD_3CN, 25 °C): δ 2.88 (s, 3H), 6.65 (ddd, 2H), 6.91 (ddd, 2H), 7.04 (m, 4H), 7.41 (t, 1H), 7.59 (dt, 2H), 7.66 (dt, 2H), 8.13 (m, 2H), 8.25 (d, 2H), 8.36 (m, 2H), 8.62 (s, 2H). ESI−FTICR MS (*m*/*z*): $[M - PF_6^-]^+$ 580.1 (calcd for $C_{32}H_{24}N_5Ru$, 580.1). Elemental anal. Calcd (%) for $C_{32}H_{24}N_5RuPF_6$: C, 53.04; H, 3.34; N, 9.67. Found: C, 52.92; H, 3.49; N, 9.51.

[(bpy)$_3$Ru-Ph-Ru(dpb)(Metpy-PI)][PF$_6$]$_3$ (Ru−Ru$_C$−PI). Prepared as described above. Ru(Metpy-PI)Cl_3 (0.035 g, 0.045 mmol) and $AgBF_4$ (0.053 g, 0.27 mmol) in acetone (10 mL). [(bpy)$_3$Ru-Ph-Hdpb][PF_6]$_2$ (0.052 g, 0.045 mmol) in 1:1 DMF:*n*-BuOH (10 mL). Purified by column chromatography on silica (eluent, 20:3:1 CH_3CN:H_2O(aq):KNO_3). Yield: 0.040 g, 45%. ^{1}H NMR (400 MHz, CD_3CN, 25 °C): δ 0.90−1.00 (m, 6H), 1.25−1.45 (m, 8H), 1.85 (m, 1H), 3.63 (d, 2H), 5.39 (s, 2H), 6.70 (ddd, 2H), 6.96 (ddd, 2H), 7.05 (m, 2H), 7.14 (m, 2H), 7.42−7.55 (m, 5H), 7.64−7.74 (m, 6H), 7.78 (m, 2H), 7.83 (m, 1H), 7.90 (m, 1H), 7.95−8.00 (m, 2H), 8.08−8.18 (m, 7H), 8.29 (d, 2H), 8.38 (s, 2H), 8.44−8.50 (m, 3H), 8.54−8.60 (m, 7H), 8.63 (d, 1H), 8.75 (s, 2H). ESI−FTICR MS (*m*/*z*): $[M - PF_6^-]^+$ 1840.6 (calcd for $C_{86}H_{68}N_{13}O_4RuP_2F_{12}$, 1840.3); $[M - 2PF_6^-]^{2+}$ 847.7 (calcd for $C_{86}H_{68}N_{13}O_4RuPF_6$, 847.7); $[M - 3PF_6^-]^{3+}$ 516.8 (calcd for $C_{86}H_{68}N_{13}O_4Ru$, 516.8). Elemental anal. Calcd (%) for $C_{86}H_{68}N_{13}O_4RuP_3F_{18} \cdot 3H_2O$: C, 50.67; H, 3.66; N, 8.93. Found: C, 50.58; H, 3.56; N, 9.08.

Results and Discussion

Synthesis. The synthesis of the new terpyridine ligands ttpy-PI (**3**) and Metpy-PI (**11**) followed the routes outlined in Scheme 1. The pyromellitimide substituted phenyl-terpyridine **3** was prepared in a condensation reaction between monoanhydride **2** and 4′-[4-(aminomethyl)phenyl]-2,2′:6′,2″-terpyridine (**1**) according to the procedures developed previously.[16c] In contrast, the initial synthesis of methylene-linked Metpy-PI (**11**) commenced with the condensation of monoanhydride **2** and aminoacetaldehyde dimethyl acetal (**4**) to give diimide **5**. The subsequent liberation of the aldehyde to furnish **6** was followed by a classical ring assembly strategy according to the Kröhnke procedure.[27] Enone **9** was prepared in two steps in modest yield from **6** and 2-acetylpyridine. A final ring-forming reaction between pyridacyl pyridinium iodide **10** and enone **9** in the presence of ammonium acetate in methanol gave Metpy-PI **11**.

Because of the low yield in the synthesis of **11**, an alternative strategy similar to the one for ttpy-PI was also developed. The synthesis of 4′-cyano-2,2′:6′,2″-terpyridine **13** was earlier reported by Potts[28] and recently by John and co-workers.[29] We preferred a palladium catalyzed cyanation reaction on easily accessible 4′-chloro-2,2′:6′,2″-terpyridine **12**[30,31] following the procedures developed by Jin.[32] The cyano-functionalized terpyridine was subsequently reduced using Pd/C under H_2 in acetic acid to give **14**. A final condensation reaction between monoanhydride **2** and **14** gave Metpy-PI in 37% overall yield starting from **12**.

The synthetic approach to the cyclometalated ruthenium(II) complexes (Figure 1) followed well-established procedures.[12] Accordingly, the prepared ligands ttpy-PI, Metpy-PI, and Metpy were each reacted with 1 equiv of $RuCl_3 \cdot 3H_2O$ in refluxing ethanol to give the monotridentate Ru(X-tpy)Cl_3 species. In situ preparations of the respective [Ru(X-tpy)(acetone)$_3$]$^{3+}$ salts in refluxing acetone with $AgBF_4$ were followed by cyclometalation in DMF:*n*-BuOH mixtures at 130 °C in the presence of 1,3-di(2-pyridyl)-benzene (Hdpb) or [(bpy)$_3$Ru−Ph-Hdpb][PF_6]$_2$. After chromatography, the desired Ru$_C$−PI, Ru$_C$−φ−PI, and Ru−Ru$_C$−PI, as well as the Ru$_C$ model complex, were isolated in 33−45% yields. All new complexes gave satisfying ESI mass spectra and showed elemental analyses in accordance with the assigned structures.

Electrochemistry. The redox potentials for all complexes were determined by cyclic voltammetry (CV) and differential pulse voltammetry (DPV) and are given in Table 1. All potentials are reported vs the $Fc^{+/0}$ redox couple. For all complexes, a reversible wave at $E_{1/2} = 0.1$ V was observed, which is typical for the $Ru^{III/II}$ couple of the cyclometalated Ru$_C$ unit.[12a] In Ru−Ru$_C$−PI, a second reversible oxidation occurs at $E_{1/2} = 0.91$ V that can be assigned to the $Ru^{III/II}$ couple of the Ru unit. This value is close to that reported previously for the [(bpy)$_3$Ru−Ph-Hdpb][PF_6]$_2$ precursor ($E_{1/2} = 0.90$ V)[10] and indicates little electronic communication between the two metal centers.[33] In the PI-containing complexes, the first reduction process is observed at $E_{1/2} = -1.2$ V, corresponding to the $PI^{0/-}$ redox couple.[14,15] The

(27) Kröhnke, F. *Synthesis* **1976**, 1−24.
(28) Potts, K. T.; Cipullo, M. J.; Ralli, P.; Theodoridis, G. *J. Org. Chem.* **1982**, *47*, 3027−3038.
(29) Veauthier, J. M.; Carlson, C. N.; Collis, G. E.; Kiplinger, J. L.; John, K. D. *Synthesis* **2005**, 2683−2686.
(30) Schubert, U. S.; Schmatloch, S.; Precup, A. A. *Des. Monomers Polym.* **2002**, *5*, 211−221.
(31) Constable, E. C.; Ward, M. D. *J. Chem. Soc., Dalton Trans.* **1990**, 1405−1409.
(32) Jin, F.; Confalone, P. N. *Tetrahedron Lett.* **2000**, *41*, 3271−3273.
(33) Ward, M. D. *Chem. Soc. Rev.* **1995**, *24*, 121−134.

Scheme 1 [a]

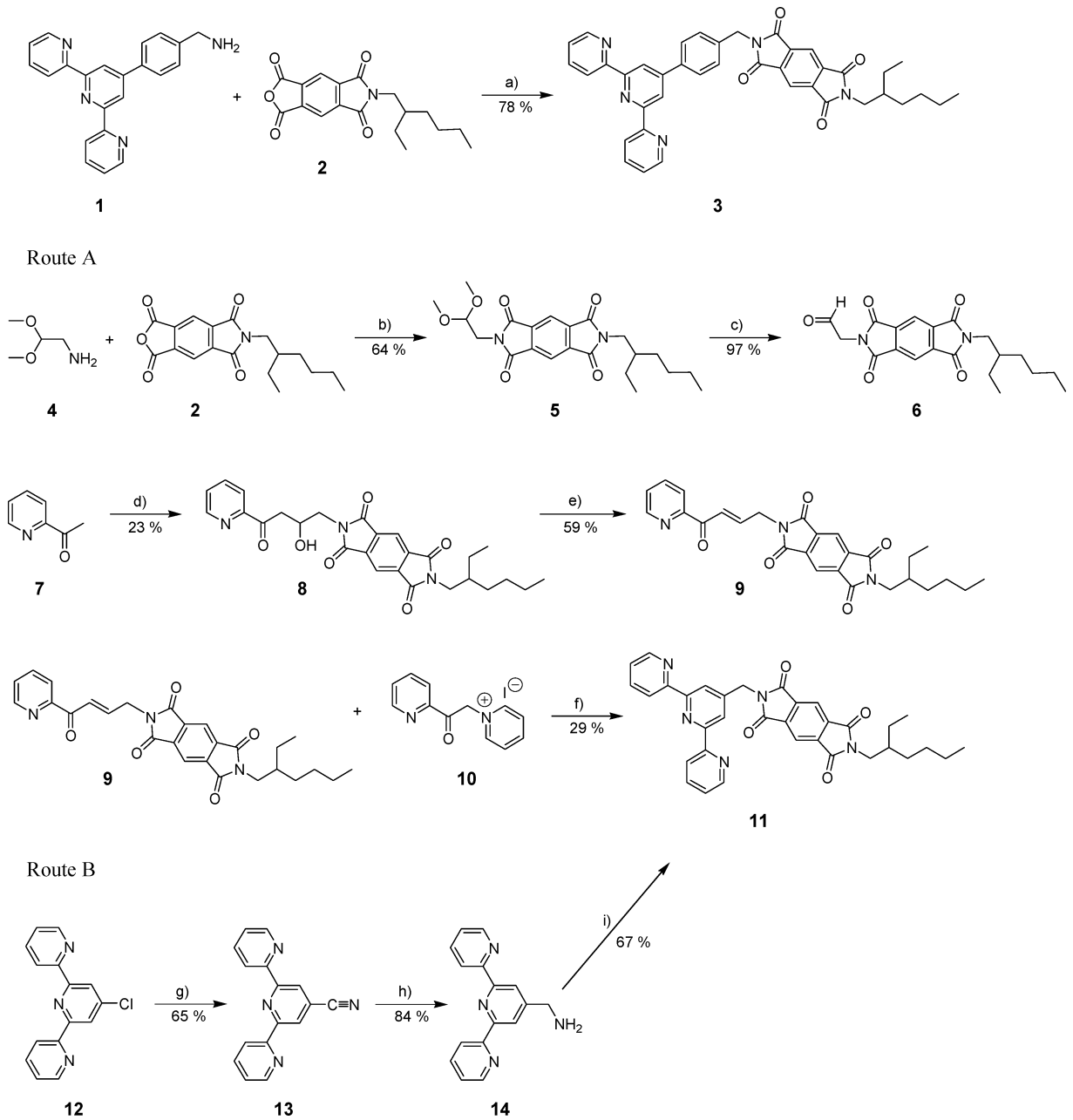

[a] (a) Toluene (reflux); (b) toluene (reflux); (c) (1) CF_3COOH (rt), (2) $NaHCO_3$; (d) (1) LDA, THF (−50 °C), (2) **6** (−78 °C); (e) MsCl, NEt_3, CH_2Cl_2 (−30 °C); (f) NH_4OAc, MeOH (reflux); (g) $Zn(CN)_2$, $Pd(dba)_2$, dppf, Zn, DMA (180 °C, microwave); (h) Pd/C, H_2, AcOH (rt); (i) **2**, toluene (reflux).

Table 1. Redox Potentials of Mono- and Bimetallic Complexes

	$E_{1/2}$ (V)[a]				
complex[b]	$Ru^{III/II}(N_6)$	$Ru^{III/II}(N_5C)$	$PI^{0/-}$	$PI^{-/2-}$	$L^{0/-}$
$Ru_C-\varphi-PI$		+0.13	−1.21	−1.80[c]	−1.90[c]
Ru_C-PI		+0.13	−1.21	−1.81	−1.99
$Ru-Ru_C-PI$	+0.91	+0.14	−1.20		−1.69[c]
Ru_C		+0.10			−1.97
$Ru_C-\varphi$[d]		+0.10			−1.99
$[Ru(bpy)_3]^{2+}$ [e]	+0.88				−1.74
$[Ru(ttpy)_2]^{2+}$ [e]	+0.84				−1.65

[a] Vs. $Fc^{+/0}$, CH_3CN, 0.1 M $TBAPF_6$. [b] As PF_6^- salts. [c] Irreversible, DPV peak potential, assigned to $PI^{-/2-}$ and bridging ligand reductions. [d] See ref 12a. Potentials reported vs. SCE, recalculated by subtracting 0.38 V. [e] See ref 16c.

second reduction of the PI unit was observed at $E_{1/2} = -1.8$ V for Ru_C-PI and $Ru_C-\varphi-PI$. In $Ru-Ru_C-PI$, however, the reduction peak arising from the $PI^{-/2-}$couple is obscured because of adsorption processes that occur around −1.7 V, where the acceptor moiety as well as the ditopic ligand of the bimetallic complex are reduced.[10] A third reduction occurs at $E_{1/2} = -1.90$ and −1.99 V for $Ru_C-\varphi-PI$ and Ru_C-PI, respectively, which can be assigned to the terpyridine ligands by comparison to the Ru_C and $Ru_C-\varphi$ model complexes.

Absorption Properties. Absorption spectra for all new complexes were obtained in CH_3CN, and the absorption maxima for the metal-to-ligand charge-transfer (MLCT) bands are listed in Table 2, together with the data for the model complexes. The PI unit gives no contribution in the wavelength region of the MLCT bands; the monometallic

Table 2. Photophysical Data (298 K)

	absorption		photophysical data				
complex[a]	λ_{max} (nm) ($\epsilon \times 10^{-4}$)		solvent	τ_{ems} (ps)	τ^{f}_{ET} (ps)	τ^{b}_{ET} (ps)	τ_{EnT} (ps)
$Ru_C-\varphi-PI$	507 (1.6)		CH_3CN	3300	13000	[b]	
Ru_C-PI	504 (1.3)		CH_3CN	240	180	28	
Ru_C-PI			CH_2Cl_2	290	220	64	
Ru_C-PI			toluene	1500	[b]	[b]	
$Ru-Ru_C-PI$	504 (2.5)	456 (2.6)	CH_2Cl_2	120	180	90	2.1
Ru_C	504 (1.3)		CH_3CN	4000			
$Ru_C-\varphi$	504 (1.1)[c]		CH_3CN	4500			
$[Ru(bpy)_3]^{2+}$ [d]		451 (1.4)	CH_3CN	8.9×10^5			
$[Ru(ttpy)_2]^{2+}$ [d]		490 (2.8)	CH_3CN	950			

[a] As PF_6^- salts. [b] Not determined. [c] See ref 12a. [d] See ref 16c.

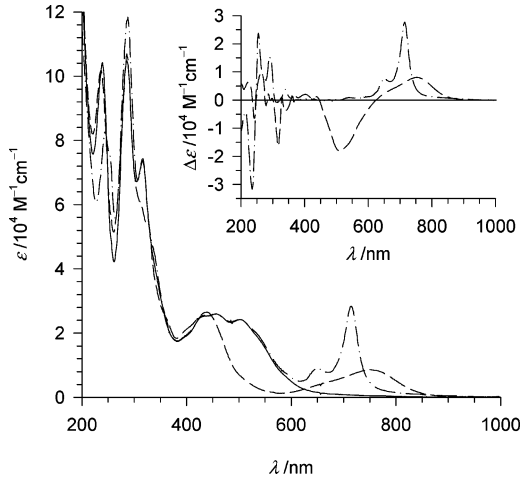

Figure 2. Absorption spectra of $Ru-Ru_C-PI$ (—), after electrolysis at 0.42 V (- - -), and at −1.48 V (-·-·-). Inset shows the corresponding difference spectra.

$Ru_C-\varphi-PI$, Ru_C-PI, $Ru_C-\varphi$, and Ru_C complexes show similar MLCT bands, with maxima around 500 nm that originate from overlapping Ru(dπ) → dpb(π*) and Ru(dπ) → tpy(π*) or ttpy(π*) transitions. However, the molar extinction coefficients are somewhat larger for the phenyl-tpy-containing complexes because of a more-delocalized excited state.[34] For both $Ru_C-\varphi-PI$ and $Ru_C-\varphi$, a shoulder is apparent at approximately 550 nm that can be assigned to Ru(dπ) → ttpy(π*) transitions, whereas the higher-energy transition (~505 nm) is due to Ru(dπ) → dpb(π*) transitions.

The $Ru-Ru_C-PI$ triad features intense MLCT transitions between 400 and 600 nm originating from both ruthenium units (Figure 2). The shape of the spectrum agreed with a 1:1 summation of the monomer spectra but with an overall magnitude of the MLCT bands that was ~30% higher, indicating that the metallic interaction increased the transition dipole moments.[10]

Spectra of the oxidized Ru_C units and the reduced PI acceptor were obtained by spectroelectrochemistry in CH_3CN solution, and the spectral changes for $Ru-Ru_C-PI$ are shown in Figure 2. The spectrum of the starting material was quantitatively recovered upon re-reduction and reoxidation, and isosbestic points were maintained in the course of electrolysis. Oxidation at 0.42 V results in bleaching of the 500 nm MLCT band of the Ru_C unit. The oxidized (Ru_C^{III}) state of the cyclometalated complex is characterized by a broad absorption band peaking at 750 nm. This band is also observed for oxidized mononuclear cyclometalated complexes[12b] and thus can be attributed to a LMCT transition rather than to an intervalence charge-transfer (IVCT) transition in the mixed-valence $Ru^{II}Ru_C^{III}$ complex. Reduction of the PI unit (−1.48 V) generates the PI radical anion and gives rise to the narrow absorption peak at 715 nm.

Energy and Electron Transfer. The monometallic $Ru_C-\varphi$ and Ru_C exhibit weak fluorescence ($\phi \approx 10^{-5}$) with ^{3}MLCT excited-state lifetimes in CH_3CN of 4.5 and 4.0 ns, respectively, as determined from time-correlated single photon counting experiments. For the $Ru_C-\varphi-PI$ dyad, the excited state was slightly quenched, with $\tau_{ems} = 3.3$ ns (CH_3CN). The only likely quenching mechanism is electron transfer to the PI unit, which has a significant driving force ($-\Delta G^0_{CS} = 0.38$ eV), as deduced from the Rehm−Weller equation taking into account the contribution from coulombic interactions (see Experimental Section). The reduced $PI^{\bullet-}$ radical could not be detected by transient absorption spectroscopy, indicating a fast recombination reaction ($Ru_C^{III}-P-PI^{\bullet-} \rightarrow Ru_C^{II}-\varphi-PI$). Earlier, we observed rapid recombination in $[Ru(bpy)_3]^{2+}-NDI$ dyads with similar linking motifs.[16c] In that study, exclusion of the phenyl unit in the bridge decreased the ratio between the rates of the recombination reaction and forward electron transfer, thus allowing for a transient population of the CS state. Applying a similar strategy in Ru_C-PI, the emission was quenched much faster, $\tau_{ems} = 240$ ps in CH_3CN, because of the shorter donor−acceptor distance. Formation of the CS state could also be detected by transient absorption pump−probe experiments with the characteristic absorption from the $PI^{\bullet-}$ radical ($\epsilon = 27\,800$ cm^{-1} M^{-1} at 715 nm). Kinetic data for the formation and decay of the CS state were obtained from a biexponential global fit at four different wavelengths and gave $\tau^{f}_{ET} = 180$ ps for the CS reaction and $\tau^{b}_{ET} = 28$ ps for the charge recombination (CR) reaction.

The CR reaction occurs in the Marcus inverted region, where the electron-transfer rate should decrease monotonically with increasing driving force ($-\Delta G^0_{CR}$) and decreasing reorganization energy (λ).[35] Because λ is expected to decrease and $-\Delta G^0_{CR}$ to increase with decreasing solvent polarity, the Ru_C-PI dyad was further investigated in CH_2Cl_2 and

(34) Collin, J.-P.; Guillerez, S.; Sauvage, J.-P.; Barigelletti, F.; De Cola, L.; Flamigni, L.; Balzani, V. *Inorg. Chem.* **1991**, *30*, 4230−4238.

(35) Marcus, R. A.; Sutin, N. *Biochim. Biophys. Acta* **1985**, *811*, 265−322.

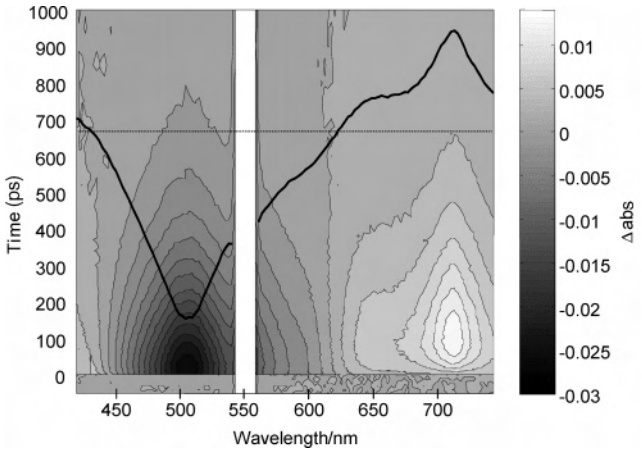

Figure 3. Transient absorption data for Ru_C−PI showing the excited-state recovery around 510 nm and the formation and decay of the $PI^{\bullet-}$ radical around 715 nm. The overlaid line is the transient spectra recorded after 125 ps (excitation at 550 nm, CH_2Cl_2).

toluene. Time-resolved emission measurements in CH_2Cl_2 showed fast emission quenching (τ_{ems} = 290 ps), although not as fast as in CH_3CN (τ_{ems} = 240 ps), whereas in toluene, the emission was not quenched at all (τ_{ems} = 1.5 ns for both Ru_C−PI and Ru_C). The results can be explained from the difference in driving force for the CS reaction as calculated from the Rehm−Weller equation (see Experimental Section), giving a highly endothermic reaction in toluene ($-\Delta G^0_{CS}$ = −0.27 eV).

The calculations further predict a larger driving force for the CR reaction in CH_2Cl_2 ($-\Delta G^0_{CR}$ = 1.40 eV) as compared to CH_3CN ($-\Delta G^0_{CR}$ = 1.26 eV), and the Marcus theory thus predicts CH_2Cl_2 to be the better solvent with respect to forming a high transient population of the Ru_C^{III}−$PI^{\bullet-}$ state. Transient absorption experiments of Ru_C−PI in CH_2Cl_2 gave τ^f_{ET} = 220 ps and τ^b_{ET} = 64 ps. Figure 3 shows the appearance of the CS state in CH_2Cl_2, in which the $PI^{\bullet-}$ radical absorption around 715 nm reached a maximum after ∼125 ps. Around 510 nm, the negative signal from the ground-state bleach of the ^{1}MLCT state is apparent. With a consecutive mechanism, the maximum population of the CS state is 11% in CH_3CN and 18% in CH_2Cl_2. These CS concentrations are in good agreement with the CS yields obtained from transient absorption data quantified with known extinction coefficients. Because the highest transient concentration of the Ru_C^{III}−$PI^{\bullet-}$ state was observed in CH_2Cl_2, this solvent was used for further studies on the Ru−Ru_C−PI triad.

Similar to the situation in the Ru_C−PI dyad, the Ru_C-based emission in the Ru−Ru_C−PI triad is strongly quenched by the appended PI acceptor with an excited-state lifetime of 120 ps in CH_2Cl_2. Upon excitation at 550 nm, the Ru_C unit is selectively excited, whereas a 450 nm pump excites the Ru and Ru_C units in a 40:60 ratio. Figure 4 shows the transient absorption spectra immediately after excitation of Ru−Ru_C−PI at both wavelengths. A relaxed ^{3}MLCT excited state on the Ru_C unit is formed on the time scale of the 550 nm excitation pulse (fwhm ≈ 150 fs). When 450 nm excitation is used instead, the initial spectrum is reminiscent of the above but with a lower amplitude of the Ru_C ^{3}MLCT

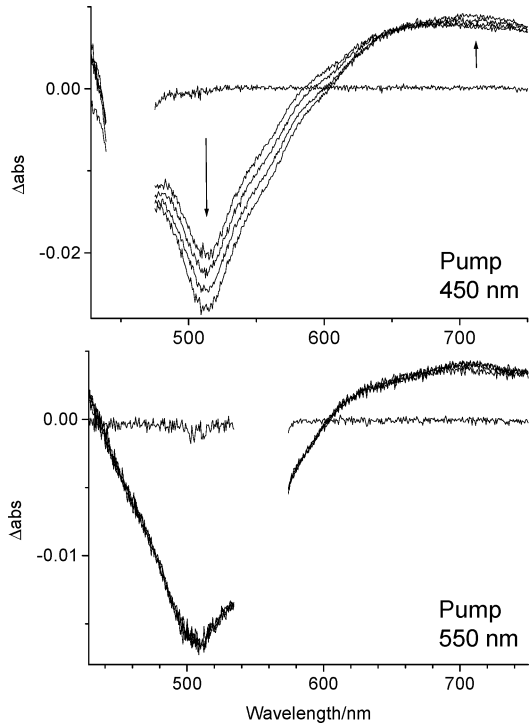

Figure 4. Transient absorption spectra for Ru−Ru_C−PI pumped at 450 or 550 nm and measured at 0.5, 1.5, 3, and 5 ps after excitation. The induced dynamics observed with a 450 nm pump are absent with a 550 nm pump (CH_2Cl_2).

excited-state signal. The amplitude then increases during the first picoseconds, as observed in similar Ru^{II}−Ru_C^{II} dyads.[10] In analogy with the results for the Ru^{II}−Ru_C^{II} dyads,[10] we ascribe this process to exchange-energy transfer from the Ru to the Ru_C unit, resulting in a population of the lowest excited state that is localized toward the PI acceptor. This is evidenced by the similarities of the transient absorption spectra for Ru−Ru_C−PI (Figure 4) and that for Ru_C−PI recorded at picosecond time scales (spectrum not shown). A single-exponential function with a time constant of τ_{EnT} = 2.1 ps convoluted with a Gaussian function with fwhm of 150 ps gave a good fit to the experimental data at 510 nm, probing the energy-transfer rate (Figure 5a,b).

In Figure 5c,d, the kinetic traces for Ru−Ru_C−PI are shown on a longer time scale. The decay of the ^{3}MLCT excited state is probed at 510 nm, whereas the $PI^{\bullet-}$ radical can be followed at 650 and 715 nm. The $PI^{\bullet-}$ radical is formed and decays again with the same kinetics, regardless of excitation wavelength (τ^f_{ET} = 180 ps and τ^b_{ET} = 90 ps). In summary, the Ru−Ru_C−PI triad functions as a combined energy-collection/charge-separation device, and the total absorption cross section for the triad leading to charge separation increases with ∼300% compared to the Ru_C−PI dyad lacking the antenna.

The maximum concentration of the Ru^{II}−Ru_C^{III}−$PI^{\bullet-}$ CS state (∼30%) in Ru−Ru_C−PI was reached after 125 ps. A subsequent excitation of the Ru unit at this time could in principle result in a second charge-transfer reaction ($^*Ru^{II}$−Ru_C^{III}−$PI^{\bullet-}$ → Ru^{III}−Ru_C^{II}−$PI^{\bullet-}$), forming a CS state with as much as 2.12 eV of potential energy stored. As a consequence of the increased distance between the charge

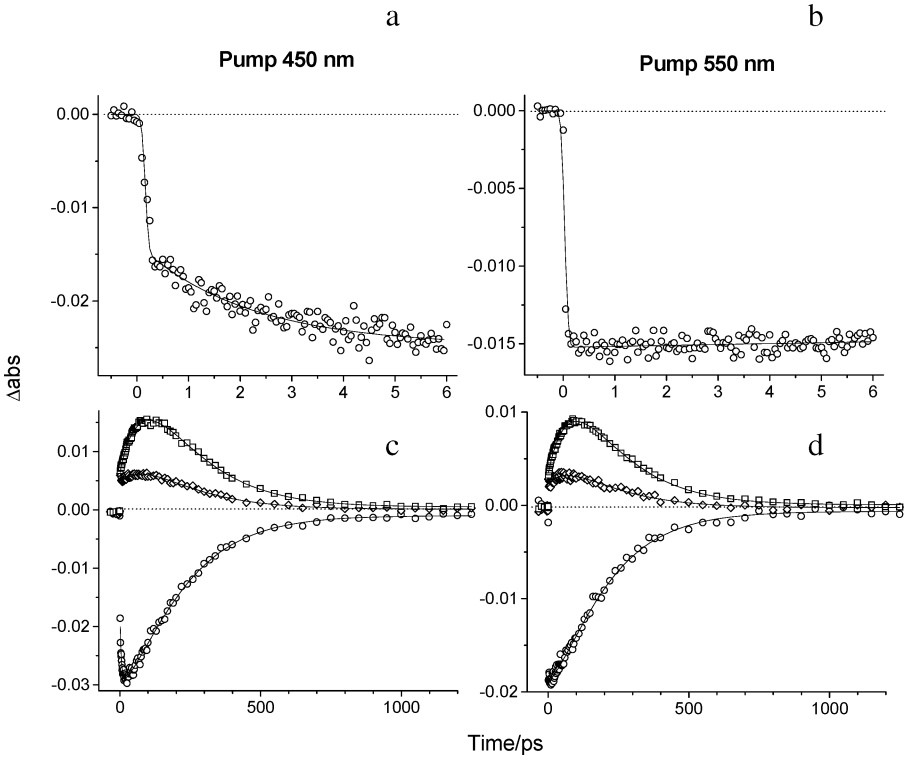

Figure 5. Transient absorption kinetic traces for Ru−Ru_C−PI in CH_2Cl_2 pumped at 450 or 550 nm and probed at 510 nm (circles), 650 nm (diamonds), and 715 nm (squares). The data show how 450 nm excitation initiates energy transfer (τ_{EnT} = 2.1 ps) between the ruthenium units (a and b). For the electron-transfer reaction (τ^f_{ET} = 180 ps and τ^b_{ET} = 90 ps), the same dynamics are observed regardless of pump wavelength (c and d).

pair, the fully CS state presumably has a longer lifetime than the initial Ru^{II}−Ru_C^{III}−$PI^{\bullet-}$ state. It would then be possible to detect this new state by transient absorption techniques at times when the primary Ru^{II}−Ru_C^{III}−$PI^{\bullet-}$ CS state has fully relaxed. The corresponding pump−pump−probe experiment was performed in CH_2Cl_2 with 450 nm excitation and an energy of 2.5 and 1 μJ for the first and second pulses, respectively. On the basis of the known extinction coefficient for the $PI^{\bullet-}$ radical, it was calculated that ca. 20% of the complex is excited by the first pulse; this leads to a maximum population of the CS state after 125 ps, which is 6% of the total irradiated sample. Taking into account the lower laser intensity and the lower extinction coefficient for the Ru^{II} unit compared to the Ru_C^{II} unit, we calculated that a second pulse would (if the mechanism works with 100% yield) convert 4% of the transiently populated CS state into the secondary CS state, Ru^{III}−Ru_C^{II}−$PI^{\bullet-}$. Thus, ca. 0.25% of the initially irradiated sample could in principle undergo the desired reaction under these experimental conditions. Assuming that the fully CS state is formed with this yield, a transient absorption signal higher than 1×10^{-3} absorption units is expected. This is higher than the noise level that lies below 0.5×10^{-3} absorption units. Unfortunately, no absorption signal from the $PI^{\bullet-}$ radical could be observed at a time scale longer than that of the Ru^{II}−Ru_C^{III}−$PI^{\bullet-}$ state. Because of the lack of a unique absorption from the two photon products, we cannot expect to see them on shorter time scales (<200 ps), as they will be masked by the transient absorption induced by single-photon excitations.

The lack of a long-lived Ru^{III}−Ru_C^{II}−$PI^{\bullet-}$ signal can have a number of possible explanations. One trivial explanation is that the charge-shift reaction (*Ru^{II}−Ru_C^{III}−$PI^{\bullet-}$ → Ru^{III}−Ru_C^{II}−$PI^{\bullet-}$) is slower than the charge recombination (Ru^{II}−Ru_C^{III}−$PI^{\bullet-}$ → Ru^{II}−Ru_C^{II}−PI). Alternatively, rapid energy transfer from the *Ru^{II} to Ru_C^{III} might occur, which would presumably be followed by a rapid deactivation of the excited Ru_C^{III} unit. The Förster energy-transfer rate constant was estimated to be less than 1×10^{10} s^{-1} and can thus be neglected. However, the low energy absorption of Ru_C^{III} indicates that Dexter energy transfer is a possible deactivation mechanism following the second excitation. For future design with similar bichromophoric motifs, it will be important to optimize the initial CS reaction to increase the transient population of the CS state. This would enhance the possibilities of answering the questions regarding the photochemical events induced by the second excitation pulse.

Conclusions

The novel Ru_C−PI, Ru_C−φ−PI, and Ru−Ru_C−PI complexes have been synthesized and characterized and their photophysical properties have been investigated in view of photoinduced charge separation. It has been shown that the strongly reducing $PI^{\bullet-}$ radical can be generated from the excited state of the cyclometalated Ru_C chromophore. Comparing the Ru_C−PI and Ru_C−φ−PI dyads, we find that the oxidative quenching is 2 orders of magnitude faster in the former complex with the shorter methylene link. With Ru_C−PI, the Ru_C^{III}−$PI^{\bullet-}$ CS state could be detected, which was not possible for Ru_C−φ−PI because of rapid charge recombination.

In Ru−Ru_C−PI, the corresponding Ru^{II}−Ru_C^{III}−$PI^{\bullet-}$ CS state is formed independently of the excitation wavelength.

This relies on the rapid energy transfer from the Ru to Ru_C chromophore. Thus, the triad works as a combined antenna/charge-separation device with an increased integrated extinction coefficient, leading to charge separation. Attempts to detect further charge separation by excitation of the Ru unit with a second photon ($^{*}Ru^{II}-Ru_C^{III}-PI^{\bullet -} \rightarrow Ru^{III}-Ru_C^{II}-PI^{\bullet -}$) in pump−pump−probe experiments were unsuccessful. Because of the appealing energetic properties of such two-photon-based charge-separated states, we will continue to investigate similar bichromophoric systems.

Acknowledgment. This work was supported by the Swedish Energy Agency, the Knut and Alice Wallenberg Foundation, the Swedish Foundation for Strategic Research, the Swedish Research Council, and NEST-STRP, SOLAR-H (EU Contract 516510). J.B. acknowledges a Research Fellow Position from the Swedish Research Council, and L.H. acknowledges a Research Fellow Position from the Royal Swedish Academy of Sciences.

IC060121L